JOURNAL OF PROPULSION AND POWER
Vol. 20, No. 4, July–August 2004

Effect of Static and Dynamic Misalignment on Ball Bearing Radial Stiffness

Bugra H. Ertas*
Texas A&M University, College Station, Texas 77840
and
John M. Vance†
Texas A&M University, College Station, Texas 77843

The primary objective was to determine, through experimental testing and rotordynamic computer simulations, the radial stiffness of an angular contact ball bearing with inner race static misalignment and outer race dynamic misalignment under various axial loads. Two different testing methods were used to determine the radial stiffness of the ball bearing: 1) eigenvalue frequency analysis and 2) critical speed transition tests. Each method used experimental measurements in conjunction with computer simulation to determine the radial ball bearing spring rate. Experimental measurements of the forward eigenvalues, backward eigenvalues, backward critical speeds, and forward critical speeds were matched with computer model simulations to determine the stiffness values for each of the cases. The rotordynamic characteristics of the rotating assembly suggested significant nonlinearity of the test bearings and also revealed signs of bifurcation for higher degrees of static misalignment.

I. Introduction

ANGULAR contact ball bearings are used in many aerospace and aircraft applications due to their load carrying capacity, durability, and low friction. They are designed to support combined loading from the axial and radial directions by incorporating a contact angle between the balls and races that usually varies between 0 and 40 deg (Ref. 1). One important characteristic of an angular contact ball bearing is the amplitude-dependent nonlinear stiffness.

The nonlinear radial stiffness of a ball bearing becomes significant when critical speeds of hard-mounted rotating assemblies are evaluated. Most aircraft gas-turbine engines utilize soft supports with fluid-type dampers surrounding the bearing in efforts to improve the rotordynamic performance, but liquid rocket engine turbopumps use hard or very stiff supports. Cryogenic rocket engines incorporate hard-mounted ball bearings in the turbopumps due to the lack of substantial damping in the bearing supports and required rotor-housing tip clearances. Extreme high and low operating temperature conditions in cryogenic fuel pumps would freeze/vaporize lubricating fluids and transform elastic seals or conventional dampers to brittle components. The combination of hard mounts and lack of lubricating fluids yield an engine with poor damping and significant rotor bending near critical speeds. For a machine of this type, knowledge of the location of the operating speed relative to the critical speed becomes imperative, making the bearing stiffness a major factor for successful operation.

Figure 1 shows this type of turbopump. It has two hard-mounted single row angular contact symmetric split inner race ball bearings, one at the pump end and one at the turbine end. Detailed views of the mounting configurations are shown in Fig. 2. The pump end bearing is used to locate the rotor and the turbine end bearing is allowed to float axially by the use of an axial preload spring. Axial preload springs are used to avoid skidding, improve shaft-positioning accuracy, decrease bearing noise, and to increase bearing fatigue life.[2] The preload spring is also compliant to axial growth of the rotor during operation due to extreme temperature changes, and it can be used to tune the rotor critical speed by changes in the bearing radial stiffness. Two hydrogen turbine stages drive the fuel pump and the liquid oxygen pump through a gear. During engine sequences, the axial thrust load varies between 0 and 4.448 kN (1000 lb) and also reverses in direction. In addition to the axial load, the pump rotor is subjected to a 2.224-kN (500-lb) radial gear load from the liquid oxygen pump. These loads make the amplitude-dependent nonlinear bearing stiffness and relative critical speed difficult to pinpoint. Another complexity in the hydrogen pump is generated from the high-pressure differential across the static support propellant plate. The fluid pressure across the plate causes deformation, which creates a taper in the bore that supports the bearing carrier. The result of the bearing carrier operating on a taper causes the ball bearing outer race to misalign with respect to the inner race. This type of misalignment, which follows the rotating imbalance, is termed dynamic misalignment. Angular misalignment is one of the most important factors that affects the bearing performance.[3] Therefore, it would be in the interest of the design engineer to know the effects of axial preload and misalignment on the ball bearing radial stiffness.

The research history for experimentally determining radial stiffness values for angular contact ball bearings with misalignment has been limited. This can be attributed to the lack of a proficient analytical method to predict stiffness values for angular misalignment between races. Classical methods of Jones[4] and Harris[1] are based on a quasi-static model of the ball bearing system, which implies that the system is in steady-state motion. The incorporation of angular misalignment transforms the steady-state problem into a transient problem. With misalignment, the balls are subject to cyclic loading, due to the load zone created. The balls are not free from acceleration; in fact, they are accelerating or decelerating.[5] Misalignment can also create dead bands in the bearing, which can lead to ball skidding and slipping. Therefore, analytical predictions accounting for misalignment utilize a more generalized formulation[5] that is time consuming and computationally extensive.

Although the authors were unable to find past research that addressed bearing race misalignment effects on stiffness, some related works on experimentally determining ball bearing radial stiffness were found. Research conducted at The Rocketdyne Division, in Canoga Park, California, involved similar tests on the space shuttle main engine angular contact ball bearing. Initial testing was

Presented as Paper 2002-4160 at the AIAA/ASME/SAE Joint Power/Propulsion Conference, Indianapolis, IN, 2002; received 21 January 2002; revision received 20 January 2004; accepted for publication 22 January 2004.

*Research Assistant, Turbomachinery Laboratory, Test Cell # 136, F.M. 2818 & George Bush Drive; bugra_e@yahoo.com. Student Member AIAA.
†Professor, Mechanical Engineering Department, Mail Stop 3123; jvance@mengr.tamu.edu.

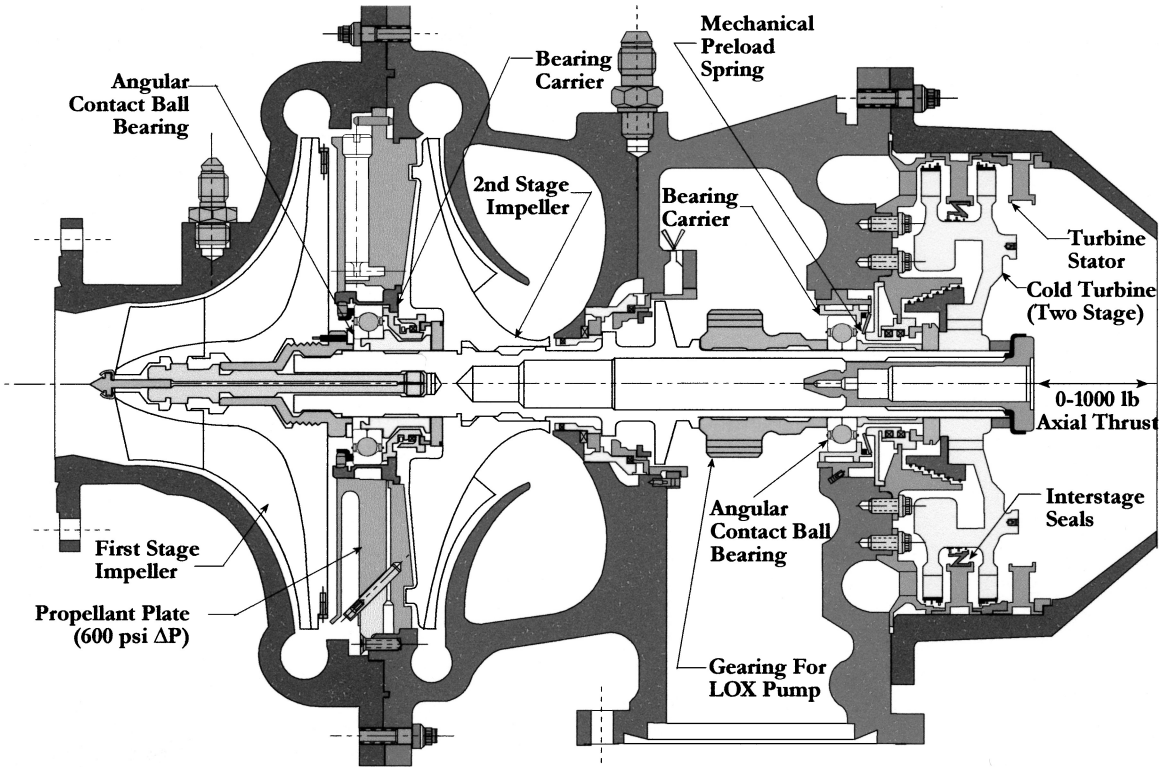

Fig. 1 Liquid hydrogen fuel turbopump.

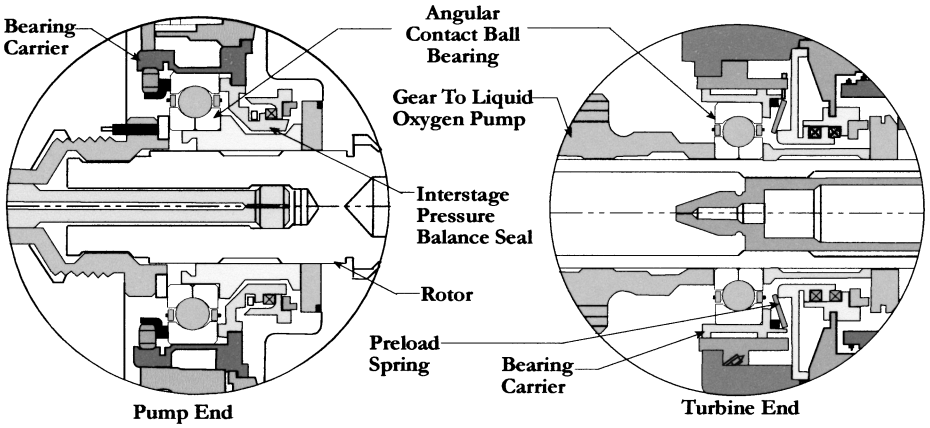

Fig. 2 Turbopump bearing mounts.

performed by Beatty and Rowan,[6] and follow-up experiments were conducted by Butner, et al.[7] Other authors who published experimental results for ball bearings are Walford and Stone.[8] Walford and Stone conducted experiments to determine the stiffness and damping characteristics for a pair of 60-mm-bore angular contact ball bearings without angular misalignment.

The main objective of the present work is to investigate experimentally the influence of inner race static misalignment and outer race dynamic misalignment on ball bearing radial stiffness.

II. Experimental Procedure and Test Rig Design

A. Angular Contact Ball Bearing

The test bearing used to investigate the effects of axial preload and misalignment on ball bearing radial stiffness was an angular contact ball bearing used in the pump and turbine end for the fuel turbopump shown in Fig. 1. The test bearing has a 20-deg contact angle and a symmetric split inner race. This bearing is unusual because most bearings with the same outer diameter and bore diameter contain 11 balls, but this particular bearing incorporates two extra balls for additional radial stiffness. The bearing retainer is a one-piece special alloy armored cage with fluorocarbon inserts. Experimental testing was conducted for static misalignment of the inner race and dynamic misalignment of the outer race for axial preloads of 156 N (35 lb), 356 N (80 lb), 1148 N (258 lb), and 1962 N (441 lb). Two different test rig configurations were used to collect the data.[9]

B. Static Misalignment Test Rig

The bearing test rig used for the static misalignment testing is shown in Fig. 3. Driving requirements for the test rig design were 1) to provide a stiff support for the rotor assembly, 2) to have the ability to apply a range of axial thrust loads, 3) to have a very stiff rotor with the center of mass close to the test bearing, and 4) to be able to incorporate different degrees of static misalignment of the test bearing inner race. The axial preload was applied through the pressure piston using pressurized air at 115 psi, and, to ensure that the majority of the axial thrust was transferred to the test bearing; the slave-bearing carrier was designed to slide with a diametrical clearance of 0.116 mm (0.004 in.). Friction tests were performed to

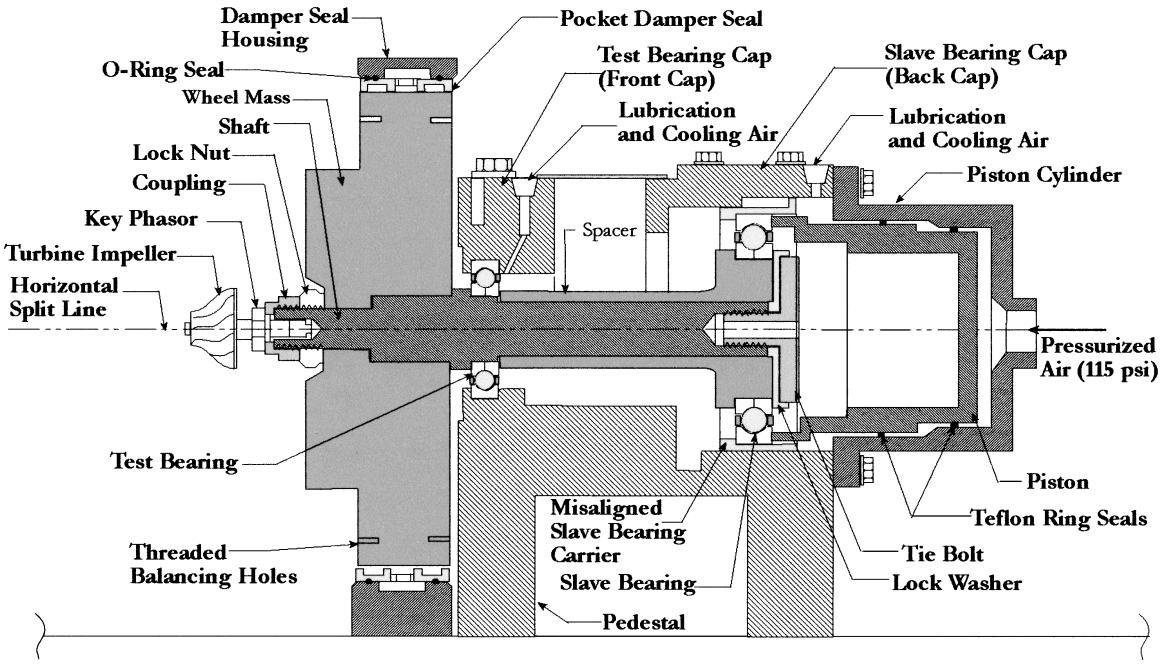

Fig. 3 Static misalignment test rig cross section.

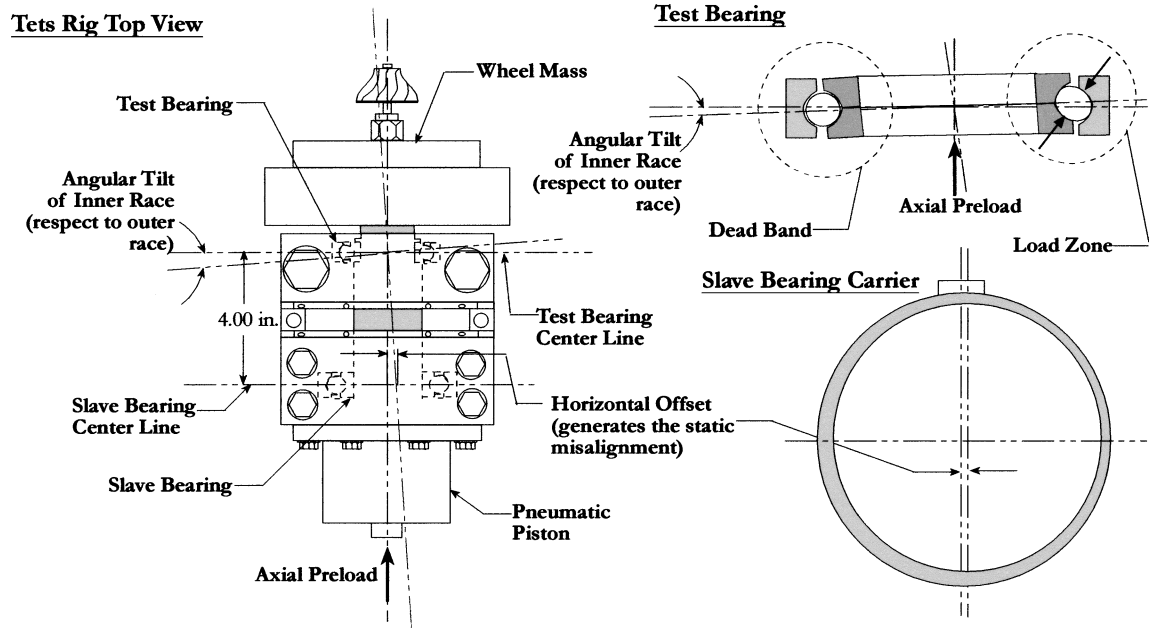

Fig. 4 Static misalignment.

determine the friction factor contributed from the Teflon® ring seals and slave-bearing carrier. Synchronous vibrations during traverse through critical speeds were kept bounded with a four-bladed pocket damper seal.[10]

The type of static misalignment produced in these tests is termed "out of line" misalignment.[1] Static misalignment of the test bearing inner race was generated by offsetting the inner bore of the slave-bearing carrier as shown in Fig. 4. Figure 4 shows a cross-sectional view of the test bearing at the horizontal split line. A top view of the test rig and a back view of the slave-bearing carrier are also shown. The horizontal offset of the slave bearing carrier's inner bore with respect to its outer surface generated an angular tilt of the test bearing inner race with respect to the outer race, which created a converging/diverging load zone centered on the left side of the bearing. Therefore, the load distribution about the circumference of the pitch circle diameter was nonuniform.

Three different degrees of static misalignment were tested: 1) 0.75 mil/in. (0.0762-mm horizontal offset or 0.0430-deg inner race angular tilt), 2) 1.50 mil/in. (0.1524-mm horizontal offset or 0.0859-deg inner race angular tilt), and 3) 3.0 mil/in. (0.3048-mm horizontal offset or 0.1719-deg inner race angular tilt. Unlike the dynamic misalignment, the orientation of the static misalignment is stationary or nonrotating.

C. Dynamic Misalignment Test Rig

A cross-sectional view of the dynamic misalignment bearing test rig is shown in Fig. 5. The dynamic misalignment was generated with the use of an axial preload spring in combination with a bearing carrier operating on a taper. To produce a pure outer race misalignment, an aligned slave-bearing carrier was used, and the test bearing donut bore was machined with a taper. The taper rate was 2 mil/in.,

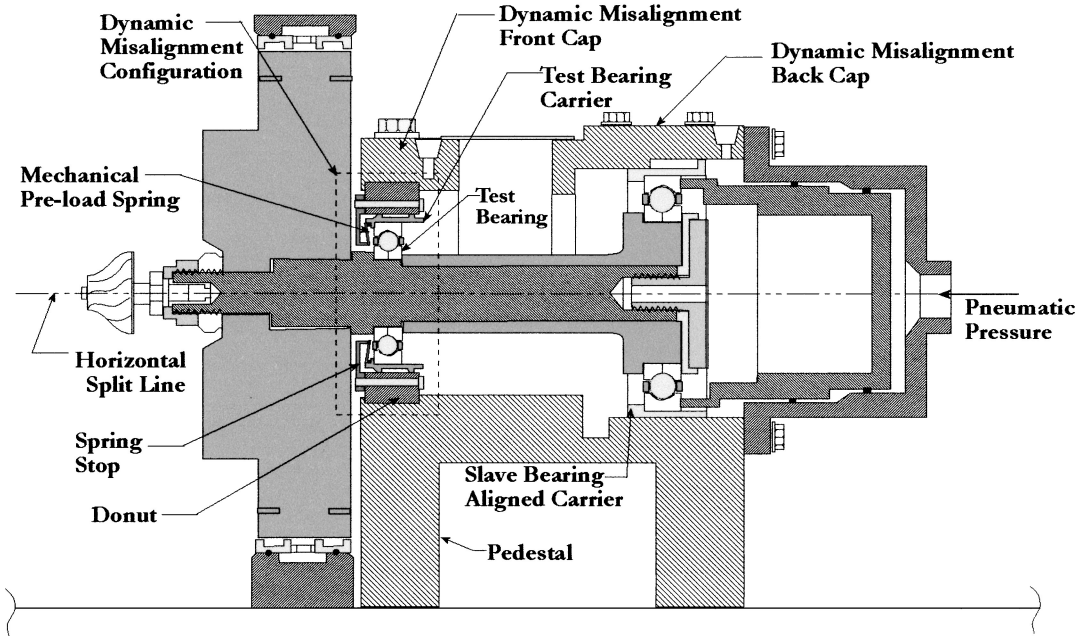

Fig. 5 Dynamic misalignment test rig cross section.

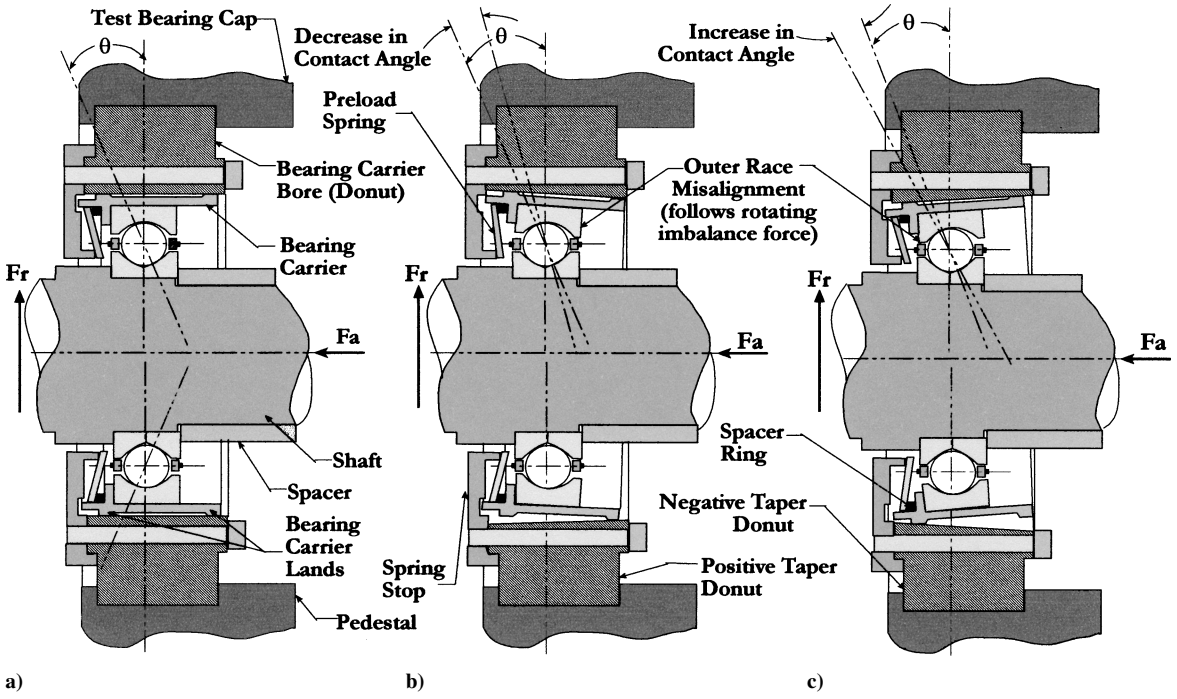

Fig. 6 Dynamic misalignment configurations: a) no taper configuration, b) positive taper configuration, and c) neagtive taper configuration.

which yields an outer race tilt angle of 0.1146 deg. The test rig in Fig. 5 incorporated a test bearing carrier, preload washer (spring), tapered donut (reversible), and a spring stop.

Two taper configurations are shown in Fig. 6. Rotating tests were conducted for a positive taper and a negative taper. The orientation of the outer race misalignment is dictated by the direction of the rotating imbalance F_r and the direction of the axial thrust F_a. The three different parts of Fig. 6 also show the change in contact angle between the outer race and balls.

D. Rotating Tests

The rotating tests were composed of eigenvalue frequency analysis and critical speed transitions. The experimental setups for the two tests are shown in Figs. 7a and 7b. The eigenvalue test setup (Fig. 7a), for modal vibration testing, utilized four essential components: 1) LDS 4408 shaker, 2) Hewlett Packard 35670A dynamic signal analyzer, 3) B&K Precision 10-Ω oscilloscope, and 4) a signal generator. Three Bently Nevada Proximity Probes were used to obtain real-time display of the whirl orbit. The whirl orbit was useful for orbit size monitoring and resonance detection during runup and coast downs. The 40-1b force shaker was used to excite the rotor natural frequencies while rotating at a constant speed. Although several types of excitation signals from the signal generator were investigated, the finalized test data were collected by the use of a periodic chirp signal with a frequency range of 400 Hz, due to the ability to produce a clean distinct peak for the frequency response. The application point of the shaker force was located 0.5 in. below the horizontal split line of the pedestal in line with the test bearing. As the test rig was being shaken, the horizontal proximity probe was

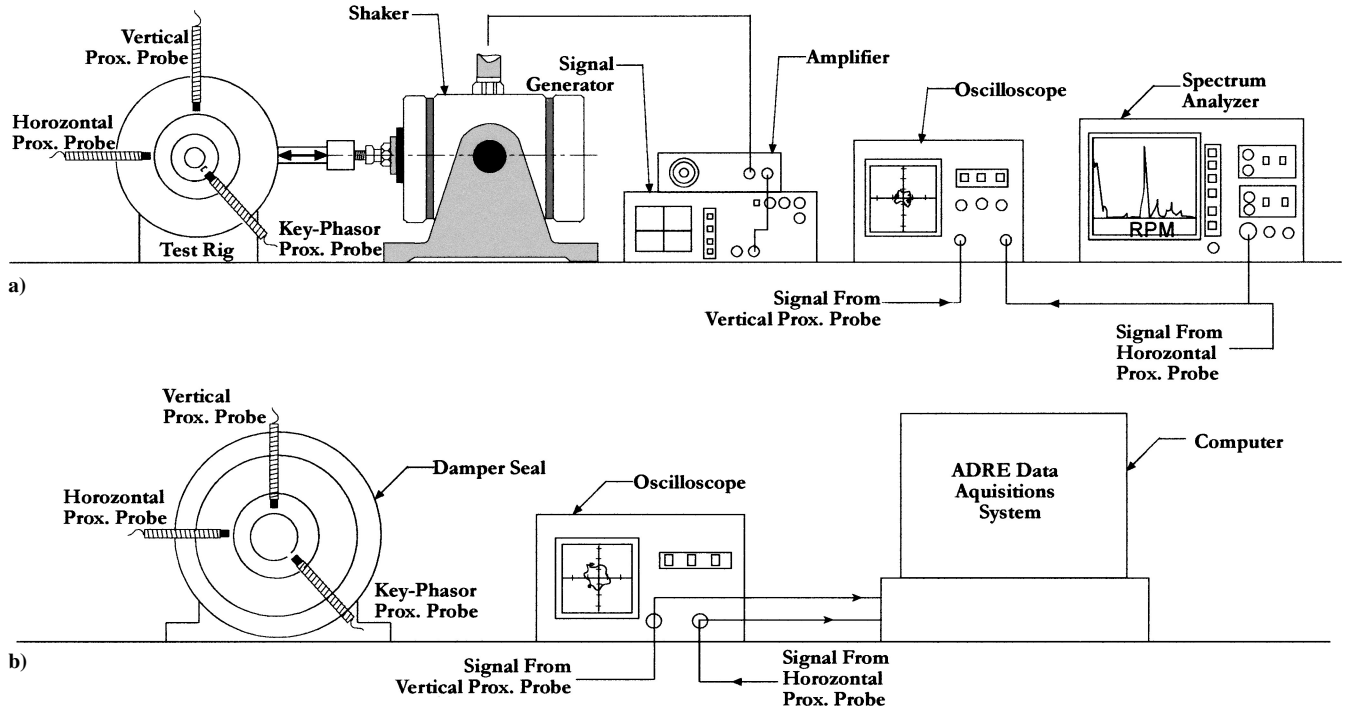

Fig. 7 Rotating test setup.

used to detect the horizontal vibration response of the rotor wheel. This signal was input into the signal analyzer, where the signals from the proximity probe were used to display the peak frequencies of the vibration response. Rotating speed of the test rig was monitored by the use of a key-phasor and data were collected for axial preloads of 0, 156, 356, 1148, and 1962 N. Note that the constant speed shaker excitation tests were only administered to the 0.75 mil/in. static misalignment case. This can be attributed to the reduction in vibration transmissibility through the bearing for larger magnitudes of angular misalignment. The recorded forward and backward eigenvalue frequencies were then used in conjunction with XLTRC[11] to determine the radial stiffness values for the test bearing.

The next sets of rotating tests were critical speed transition tests. The experimental setup in Fig. 7b shows the use of ADRE, a data acquisitions and condition monitoring system. ADRE was used to observe and record the critical speed transitions, which ranged from 6000 to 18,000 rpm. Unlike the constant speed eigenvalue shaker excitation tests, the critical speed transitions involved recording run up and coast down data, which was then displayed in the form of Bode response plots, waterfall plots, spectrum plots, and whirl orbit plots.

III. Computer Simulations

A. XLTRC Computer Model

Determination of the dynamic and static radial stiffness values required the use of experimental measurements in combination with rotordynamic computer simulations. Experimental measurements such as static deflections, forward/backward eigenvalue frequencies, and forward/backward critical speeds were matched by the use of simulations in XLTRC. The XLTRC computer model of the test rotor is shown in Fig. 8. The model is constructed from 41 discrete mass elements and has various force coefficient files linked to the rotor model at three axial locations (5.45, 7.209, and 11.093 in.). These files are associated with the pocket damper seal, test bearing, and slave bearing. The computer model for the rotor assembly was verified when experimental free–free mode natural frequencies were matched.

B. Rotordynamic Simulations

Radial stiffness values collected by experimental eigenvalue frequency spectrum measurements were determined by matching computer-simulated eigenvalues. Backward and forward eigenvalues were simulated for a range of radial spring rate values, as shown in Figs. 9 and 10, respectively, for rotor speeds of 4500 and 8500 rpm. The use of the predicted plots (Figs. 9 and 10) while experimental frequency spectrum measurements were taken (Fig. 11) proved to be an effective guide for distinguishing backward and forward eigenvalues from other significant frequency peaks in the spectrum.

To model the backward and forward critical speeds, the horizontal and vertical foundation stiffness values were accounted for. In addition, the bearing stiffness value inputs were adjusted with increasing speed to simulate the frequency seperation between the backward and forward critical speeds. The last force coefficient file used was the damper seal file. The damper seal was used to control and match rotor vibration amplitudes through critical speed transitions.

IV. Experimental Results and Discussion

A. Shaker Excitation Test Results (First Test Bearing)

The eigenvalue shaker excitation tests only address the 0.75-mil/in. static misalignment case and were only performed in the horizontal direction. Although static misalignments of 1.5 mil/in. and 3.0 mil/in. were also tested, the vibration transmissibility through the bearing was poor for these cases. It is most likely that the transmissibility problem is attributed to the increase in internal dead band clearance with the larger misalignments. The resultant resonance peaks for the larger misalignments were undetectable, especially near the synchronous frequency and its harmonics. Shaker tests were performed for speeds between 0 and 8500 rpm. Two examples of frequency spectrum data are shown in Figs. 11 and 12. Figure 11 shows the difficulty in obtaining a clean distinct frequency spectrum due to the static misalignment. Two broad band peaks are shown on either side of 13,500 rpm, which was three times running speed. The second example (Fig. 12), shows a nonrotating case at 356-N (80-lb) axial preload. For this case, the resonance peak is clearly visible at 11,600 rpm.

Several trials were averaged for each case, and the spring rate was backed out by the use of averaged eigenvalues. Bearing stiffness values varied from 70,047 kN/m (4×10^5 lb/in.) to 246,916 kN/m (1.41×10^6 lb/in.). Result plots for stiffness vs speed and stiffness vs axial preload are shown in Figs. 13 and 14. Results in Figs. 13 and 14 indicate an increasing stiffness for low speeds and a decreasing

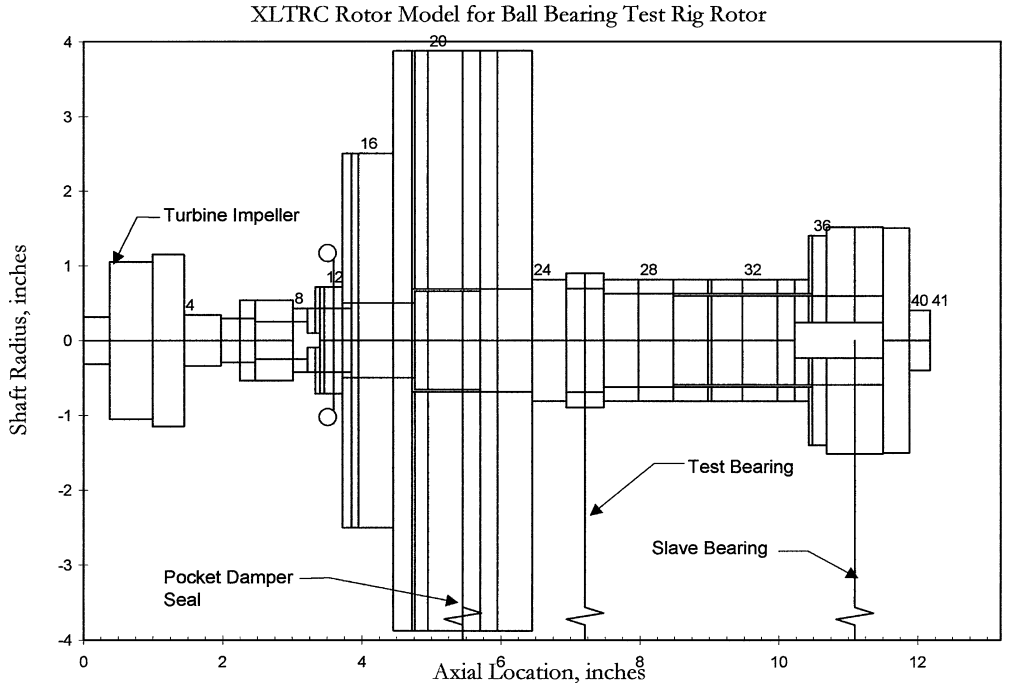

Fig. 8 XLTRC rotor model.

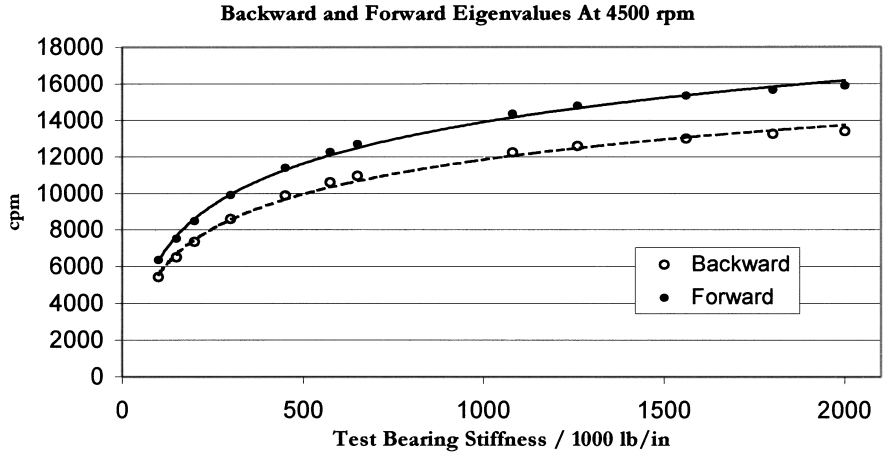

Fig. 9 Rotor eigenvalues for 4500 rpm.

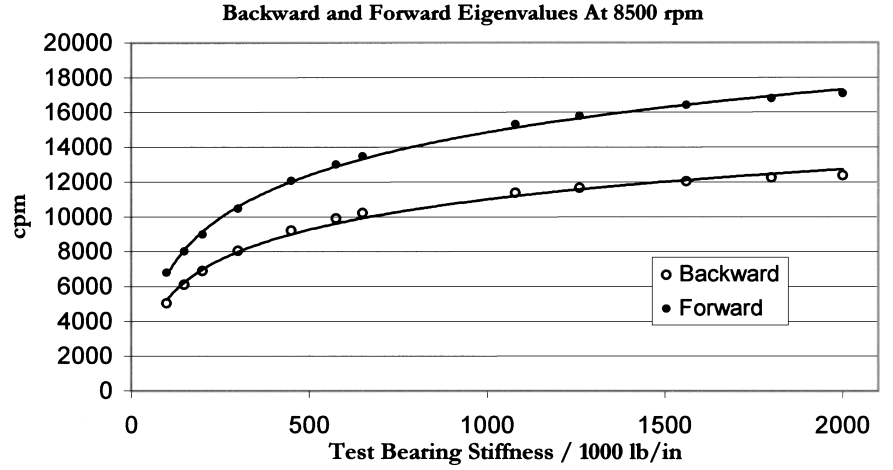

Fig. 10 Rotor eigenvalues for 8500 rpm.

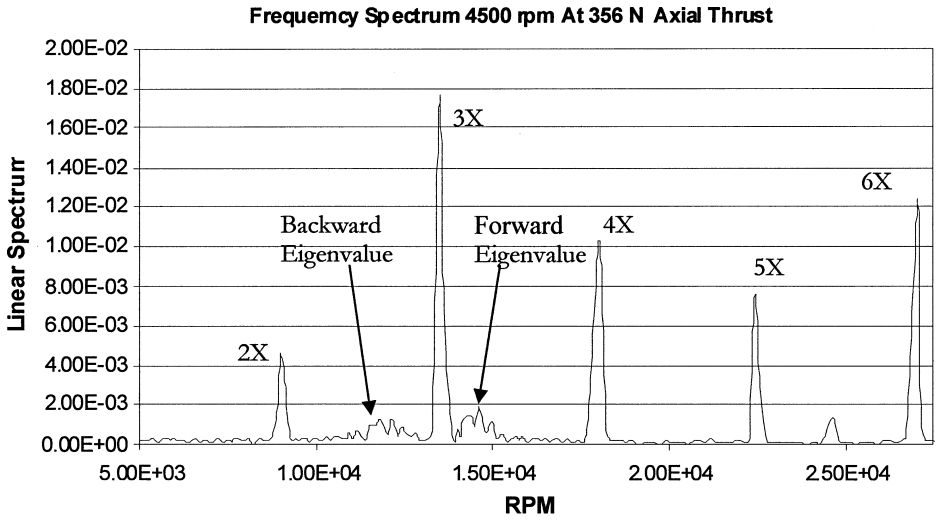

Fig. 11 Frequency spectrum 4500 rpm for axial preload 356 N.

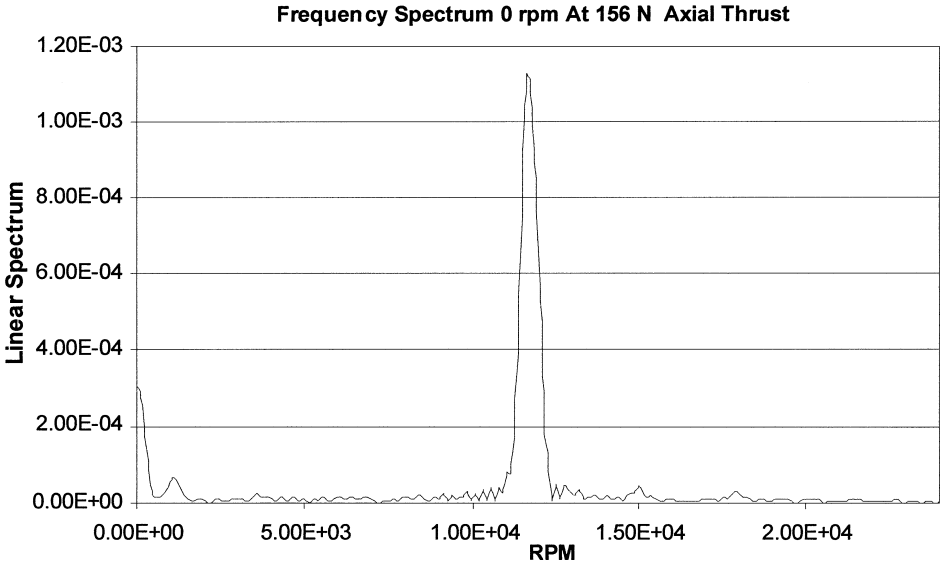

Fig. 12 Frequency spectrum nonrotating for axial preload 156 N.

stiffness at higher speed ranges. Figures 13 and 14 also show that the increase in axial preload increases the radial stiffness. There was no rotating data taken for zero axial preload.

B. Critical Speed Results (0.75 mil/in.) First Test Bearing

Two different critical speeds were observed in the Bode plots from ADRE. The first, or lower, critical speed was verified to be backward for most of the cases. Backward whirl was clearly seen by observation of the whirl orbit sequence through the critical. An example of a Bode plot and a whirl orbit sequence is shown in Figs. 15 and 16. Figure 16 shows the characteristic hardening spring effect and nonlinear jump as the rotor traverses through the critical speed at 14,000 rpm. Also note how the bearing stiffness asymmetry introduced through the static misalignment resulted in a split critical. This resulted in backward processional motion of the rotor whirl orbit, as shown in the orbit plots at 7900–8000 rpm. The synchronous backward whirl phenomenon is predicted by theory, but often is construed by practicing engineers as a theoretical anomaly that does not materialize in real-life applications. This is a misconception, as shown in this case and other rare instances with high asymmetry and low damping in the bearings/bearing supports. The ability to record transient vibration data and carefully review the rotor whirl orbits captured between the two critical speeds is key to proving this phenomenon is real and of practical value.

All critical speed data were taken from the coast down in efforts to eliminate the effects from the turbine. Stiffness vs axial preload relations for backward and forward critical speeds are shown in Fig. 17. Note that the dynamic radial stiffness (for forward critical) increases 261% for a preload range from 156 N (35 lb) to 1148 N (258 lb) when the smallest static misalignment value of 0.75 mils/in. is used. Recall that the bearing in application experiences axial thrust ranging between 0 and 4.448 N (0–1000 lb). Also, with increasing synchronous rotor speed, the backward eigenvalues decrease as the forward eigenvalues increase. These trends on the eigenvalues can be attributed to the increase in the gyroscopic moment of the wheel as rotor speed increases. Gyroscopic coupling in a rotor bearing system is destiffening for backward precession (decrease in frequency) and stiffening (increase in frequency) for forward precession.

C. Static Misalignment Critical Speed Test Results (Second Test Bearing)

After the rotating eigenvalue tests and critical speed transition tests were conducted on the initial test bearing, material wear on the inner race and outer race was visible. Another untested rocket engine bearing was used to conduct the static misalignment critical speed transition tests.

Three different degrees of static misalignment were tested: 1) 0.75-mil/in., 2) 1.5-mil/in., and 3) 3.0-mil/in. misalignment. The

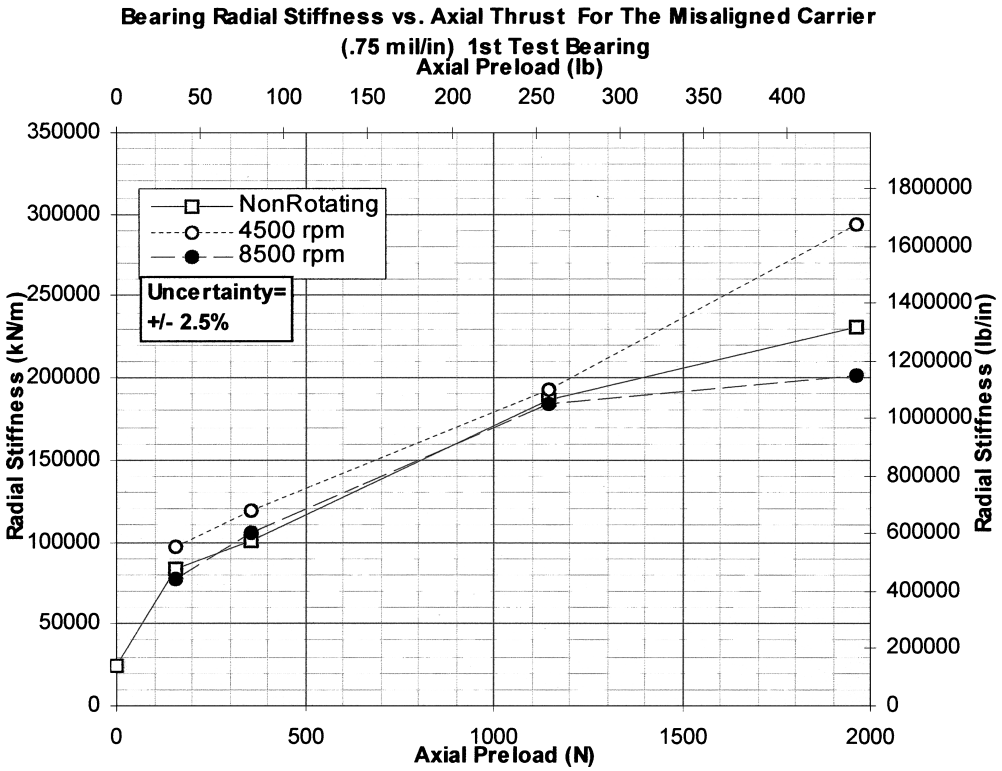

Fig. 13 Radial stiffness vs axial preload (shaker tests 0.75 mils/in.).

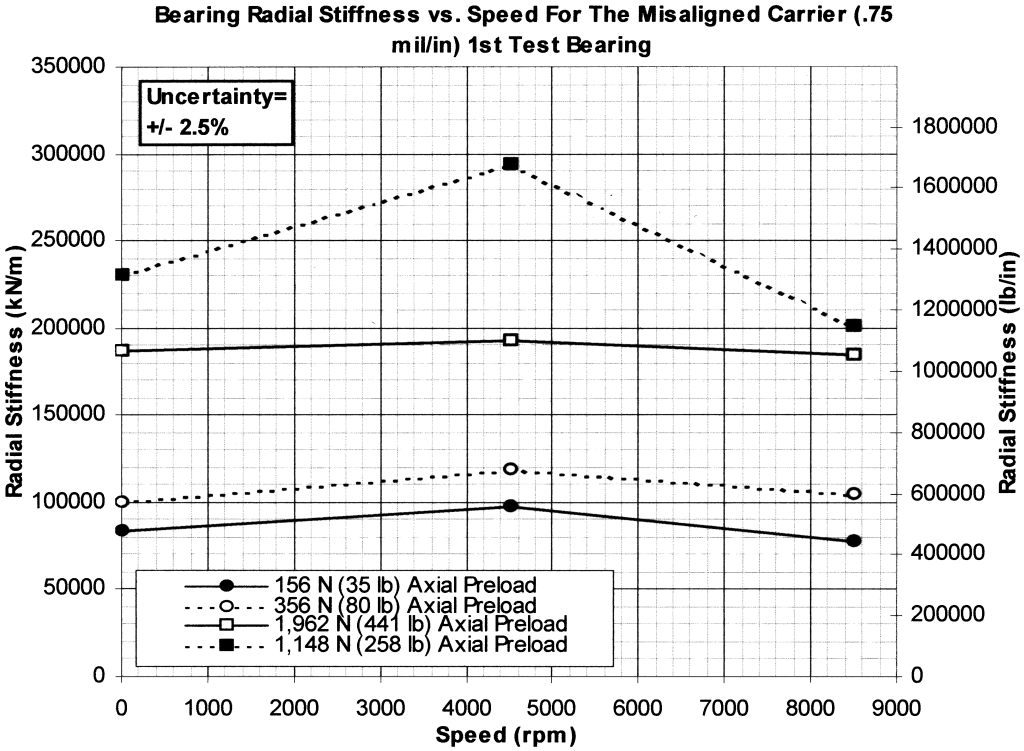

Fig. 14 Radial stiffness vs rotor speed (shaker tests 0.75 mils/in.).

stiffness increased with the increase in axial preload and inner race angular misalignment. Plots for stiffness vs axial preload for backward and forward critical speed data are shown in Figs. 18 and 19.

All three degrees of misalignment show a mixed softening and hardening behavior in the bearing. Some Bode plots depict a softening spring, whereas others show behavior of a hardening spring. This trend was true for the 0.75-mil/in. and 1.5-mil/in. misalignment cases. The 3.0-mil/in. misalignment case only behaved as a hardening spring. The general trend for stiffness values indicated an increase with inner race misalignment. Compared to the aligned (no misalignment) test, conducted by Schmidt,[12] stiffness values were lower for the 0.75-mil/in. case, but the 1.5-mil/in. and 3.0-mil/in. cases revealed higher radial stiffness values.

Most Bode plots indicated a single jump that occurs at the forward critical, but there were some response plots that had multiple jumps in orbital amplitude. The anomalies shown in Figs. 20 and 21 occur after the critical speed imbalance inversion. Also note that phase shifts are associated with the jumps in amplitude. A paper by Feng

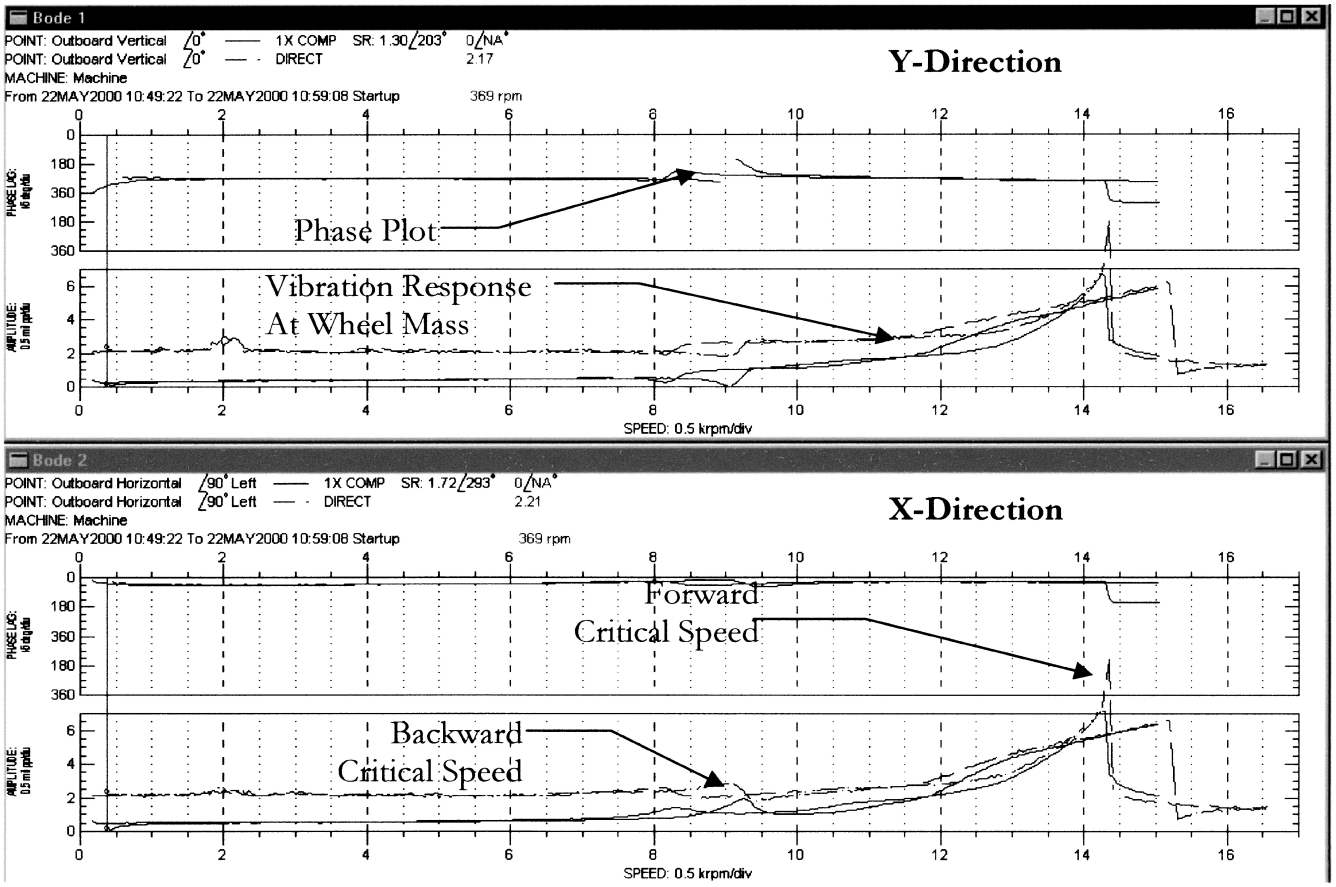

Fig. 15 Bode response plot (0.75-mil/in. and 156-N preload).

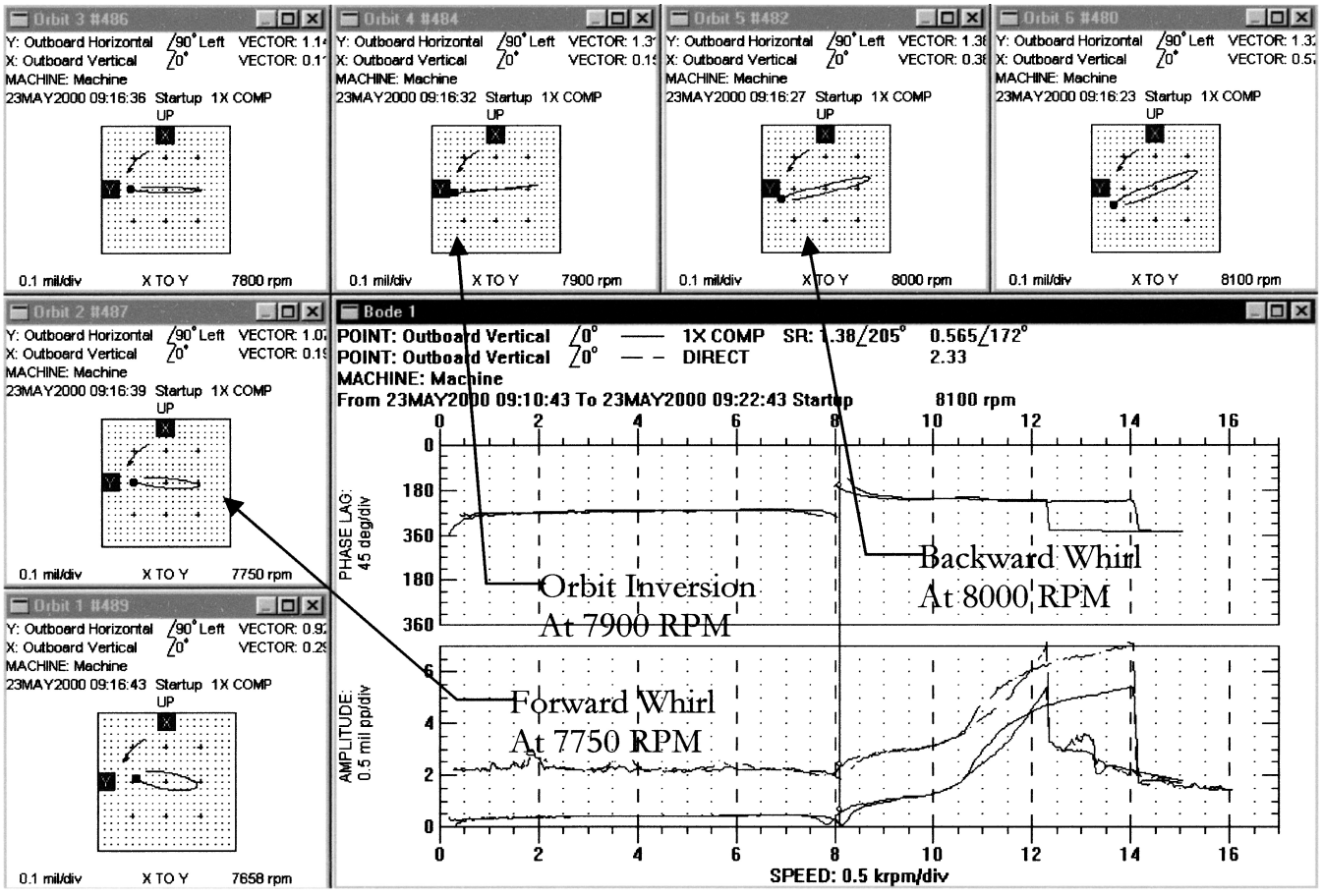

Fig. 16 Whirl orbit sequences (0.75 mil/in.).

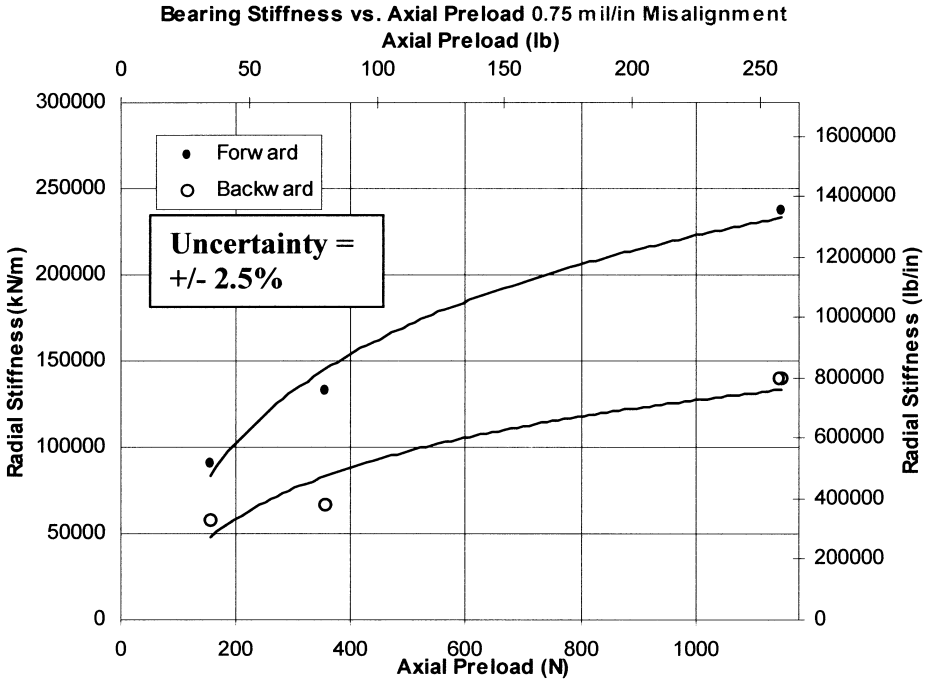

Fig. 17 Radial stiffness vs axial preload (critical speed tests 0.75 mil/in.).

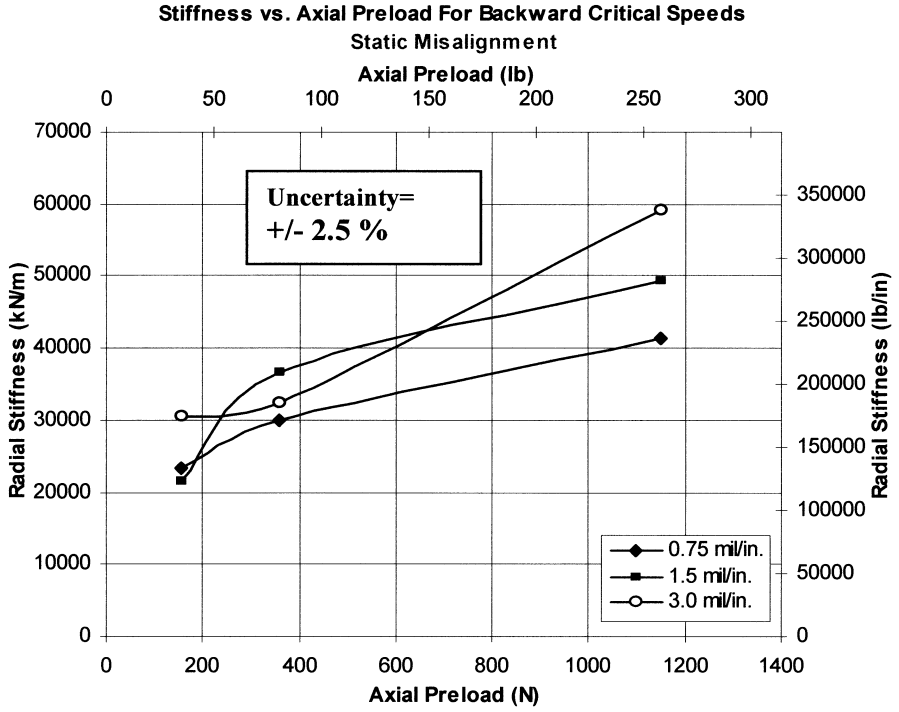

Fig. 18 Radial stiffness vs axial preload (backward whirl critical speeds, second test bearing).

and Hahn discusses possible causes for synchronous instantaneous jumps in orbital amplitudes for rotor bearing systems utilizing rolling element bearings.[13] Feng and Hahn recognize three possible sources of nonlinearity in rolling element bearings: 1) Herztian force deflection relationship inherent to spherical balls and curved races, 2) the dead band or transition fit between the bearing outer race and housing, and 3) internal radial clearance (IRC) between the balls and races, which is governed by bearing specification and the amount of preload. When a bearing operates in its IRC periods, zero contact between the balls and races can occur, which then leads to impacts and large force transmissions through the bearing. The initial peaks or jumps in Figs. 20 and 21 are associated with the nonlinear force deflection relationship between contacting components in the bearing, whereas the following jumps can possibly be explained by rotor operation within the bearing internal clearance. Feng and Hahn also discuss the range of imbalance excitation in which these jumps can occur. Yamamoto[14] also researched the effects of nonlinear behavior from rolling element bearings on rotordynamics. He analytically predicted and experimentally observed jumps in the rotor vibration response. Yamamoto found that when a rotating assembly operates within the bearing clearance, two possible solutions or types of motion are possible. The behavior of the system at this point is soley dependent on the initial conditions of the rotor–bearing system force parameters. Note that the jumps observed to this point have been synchronous in nature. Later results for the dynamic misalignment show subsynchronous jumps in orbital amplitude.

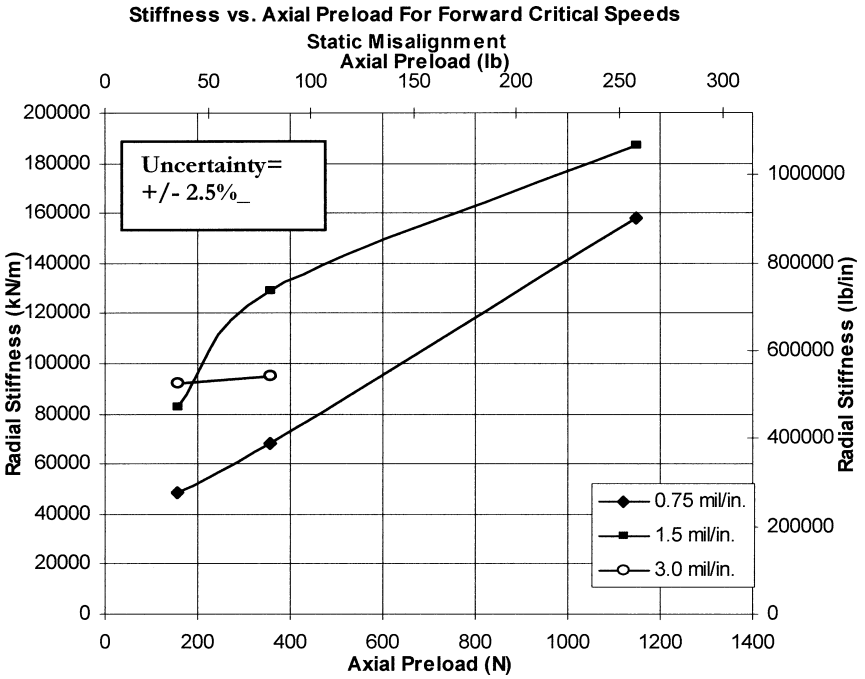

Fig. 19 Radial stiffness vs axial preload (forward whirl critical speeds, second test bearing).

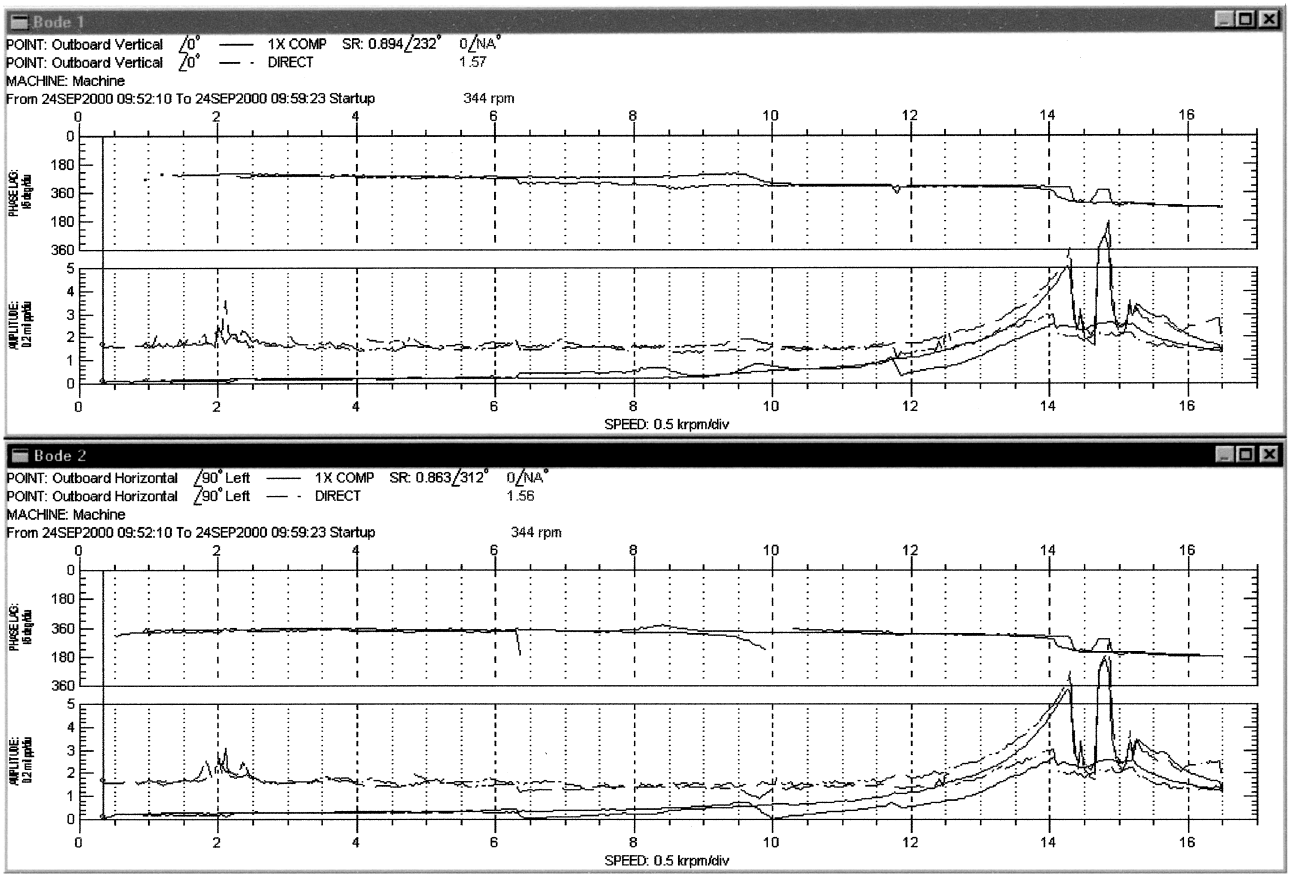

Fig. 20 Bode plot 1.5-mil/in. static misalignment 156-N preload (vibration jump).

Ball bearing radial stiffness values ranged from 21,014 kN/m (1.2×10^5 lb/in.) to 186,851 kN/m (1.067×10^6 lb/in.), depending on the misalignment and axial preload. Forward critical speeds for 3.0-mil/in. misalignment were not recorded because they resided above 20,000 rpm. Overall, the static misalignment critical speed response results are irregular and chaotic. Some cases exhibit a hardening effect in the bearing and some are softening. Several counts of bifurcation were observed throughout the experimental testing.

D. Dynamic Misalignment Critical Speed Test Results

The results for the dynamic misalignment testing are shown in Fig. 22 and show values that ranged from 17,686 kN/m (1.01×10^5 lb/in.) to 48,332 kN/m (2.76×10^5 lb/in.). Schmidt's study[12] of the same turbo pump bearing operating in an aligned bore (no taper) reports stiffness vales larger than the positive taper and negative taper stiffness values shown in Fig. 22. Schmidt measured dynamic stiffness values of 27,584 kN/m (157,518 lb/in.),

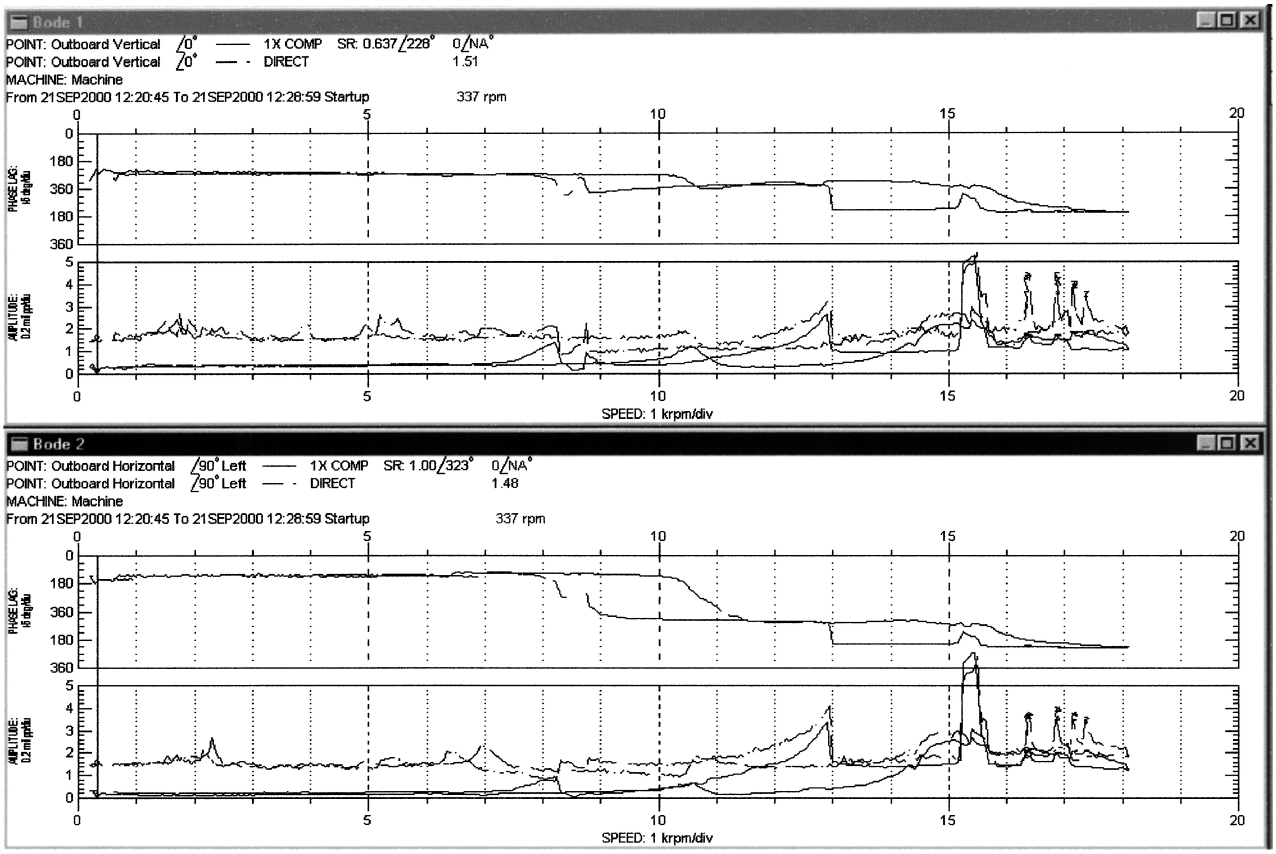

Fig. 21 Bode plot 3.0-mil/in. static misalignment 156-N preload (vibration jump).

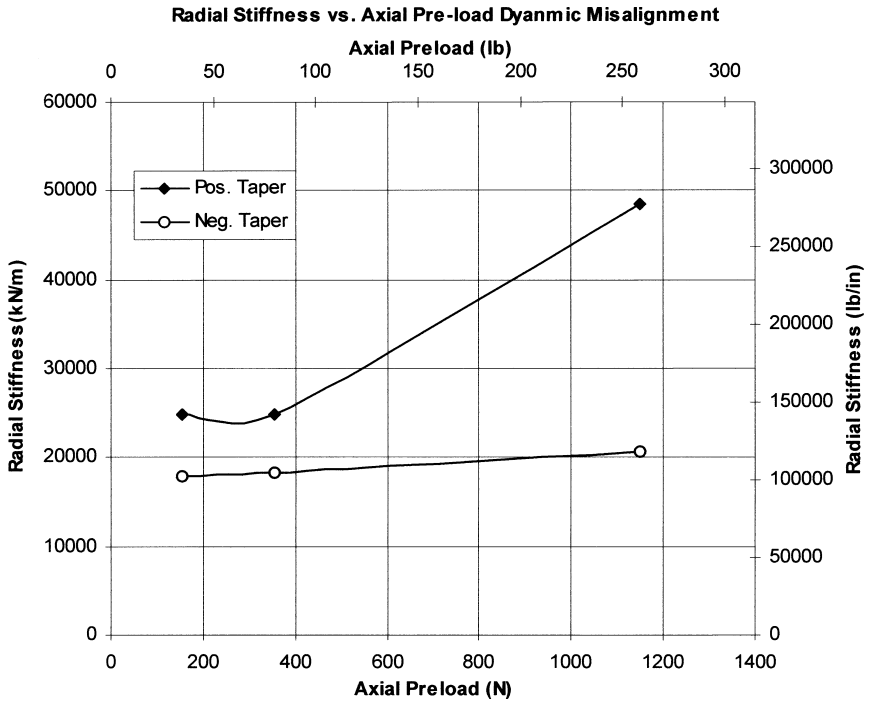

Fig. 22 Radial stiffness vs axial preload dynamic misalignment (second test bearing).

36,864 kN/m (210,511 lb/in.), and 62,000 kN/m (354,086 lb/in.) for axial preload values of 156 N (35 lb), 356 N (80 lb), and 1148 N (258 lb). Bode response plots for the positive taper revealed a softening behavior of the bearing as the rotor traversed through the critical speed, whereas the negative taper Bode plots indicated a hardening effect of the bearing. All critical speeds that were observed for the dynamic misalignment tests were forward in nature.

Response plots for the positive taper configuration did not show any asynchronous behavior during rotating tests. However, the negative taper rotating tests revealed a presence of subsynchronous frequencies for several cases. One example is shown in Fig. 23 (waterfall plot). Figure 23 shows that the rotor vibration was synchronous until after traversing through the critical speed (5750 rpm). After the critical speed inversion, the predominant vibration recorded was subsynchronous. There are two subsynchronous

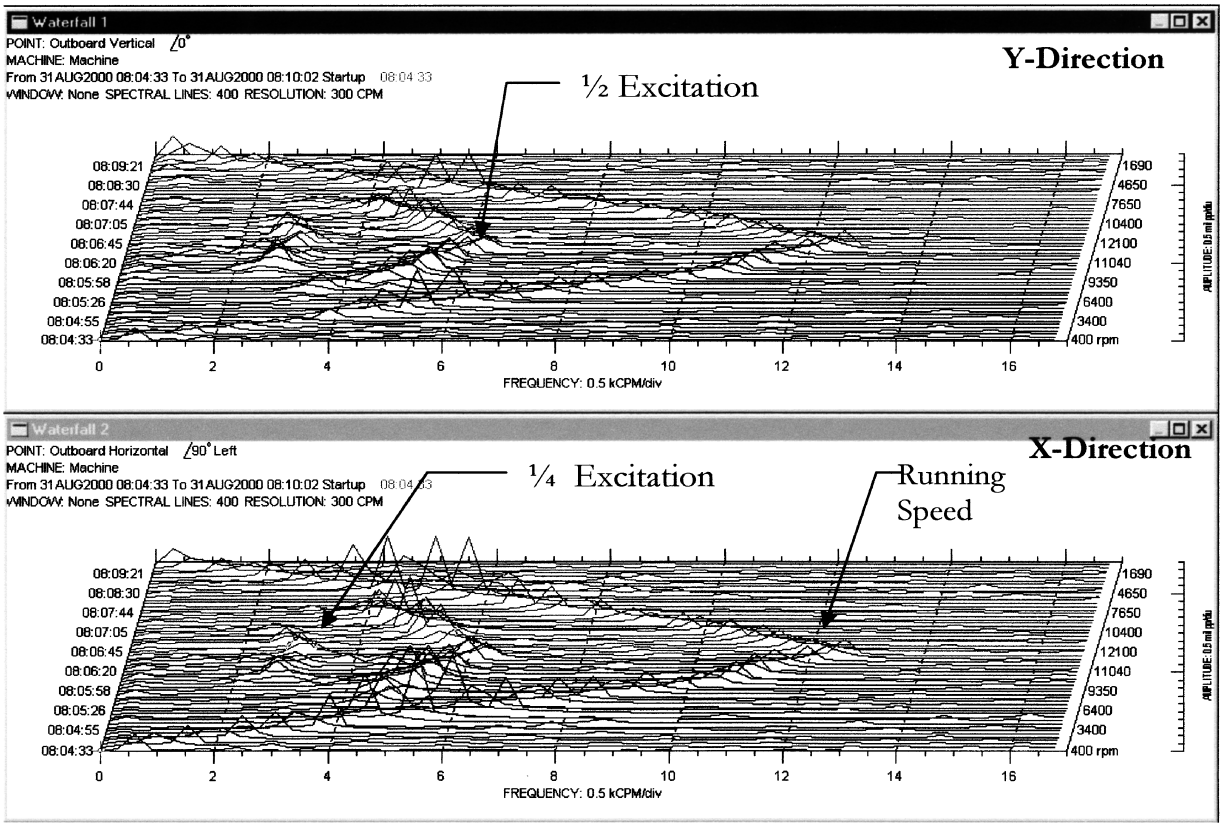

Fig. 23 Subsynchronous excitation (dynamic misalignment negative taper).

frequencies: 1) 0.5 times running speed and 2) 0.25 times running speed. The one-half frequency excitation can very possibly be a rub. Rubs in rotating assemblies produce a one-half running speed excitation that tracks the running speed.[15] The other frequency is one-quarter the running speed, and this frequency spike also tracks the running speed. Spectrum traces were used to determine the precession of the one-half and one-quarter excitations. The spectrum indicated that the one-quarter excitation was backward in nature, and this was clearly evident by comparison of the negative spectrum component with the positive spectrum component. The reverse vibration component for the one-quarter running speed is larger than the forward vibration component. The spectrum also revealed that the one-half excitation was forward in nature for all running speeds.

V. Conclusions

The primary objective of the present study was to determine, through experimental methods, the effect of static and dynamic misalignment on ball bearing radial stiffness for a range of axial preloads. The radial bearing spring rate increased with axial preload for all stiffness measurements. Static misalignment was shown to have stiffening effects on the radial stiffness, whereas dynamic misalignment lowered the radial stiffness from the aligned case.

The critical speed results for the statically misaligned hard-mounted case indicated a mixed behavior of the ball bearing stiffness nonlinearity. Both hardening and softening effects were observed during the experiments. The causes of the irregularities in the radial stiffness trends could not be established due to the inability to measure bearing conditions such as external/internal dead band, instantaneous angle of ball contact, and axial-to-radial load ratios. System anomalies were also observed for the 1.5- and 3.0-mil/in. cases. These anomalies were instantaneous jumps in the orbital amplitude after traverse through the forward critical speed. Also, static misalignment of the bearing resulted in an increase in the stiffness asymmetry, which is a necessary condition for stable synchronous backward whirl orbits in speed ranges between the peaks of a split critical.

The positive taper configuration critical speed tests indicated an increase in radial stiffness with increasing axial preload. The negative taper tests revealed subsynchronous frequency excitation with significant response amplitudes. These subsynchronous frequencies were determined to be both backward and forward whirl.

In conclusion, the radial stiffness of the test ball bearing was shown to vary between 44,880 kN/m (1×10^5 lb/in.) and 246,196 kN/m (1.41×10^6 lb/in.) for a range of axial preloads of 0–1148 N (258 lb). This study has shown that the ball bearing radial stiffness cannot be reliably predicted unless variations in axial loading, radial dynamic loading, and especially relative race misalignment are known.

Acknowledgments

The authors would like to acknowledge John Wall of Lockheed Martin Astronautics for the design of the ball bearing stiffness test rig. Sincere appreciation is also shown for Brent Schmidt for aiding with the data collection and test rig setup.

References

[1]Harris, T. A., *Rolling Bearing Analysis*, 2nd ed., Wiley Interscience, New York, 1984, pp. 180–203.

[2]Dietl, P., "Damping and Stiffness Characteristics of Rolling Element Bearings," Ph.D. Dissertation, Dept. of Mechanical Engineering, Technical Univ. of Vienna, Vienna, 1997.

[3]Gupta, P. K., "Dynamics of Rolling Element Bearings—Part IV: Ball Bearing Results," *Journal of Lubrication Technology*, Nov. 1978.

[4]Jones, A. B., "A General Theory for Elastically Constrained Ball and Radial Roller Bearings Under Arbitrary Load and Speed Conditions," *Journal of Basic Engineering*, Vol. 82, No. 2, June 1960, pp. 309–316.

[5]Gupta, P. K., "Dynamics of Rolling Element Bearings—Part III: Ball Bearing Analysis," *Journal of Lubrication Technology*, Nov. 1978.

[6]Beatty, R. F., and Rowan, B. F., "Determination of Ball Bearing Dynamic Stiffness," TR NAS8-27980, Rocketdyne Division, Canoga Park, CA, 1981.

[7]Butner, M. F., Murphy, B. T., and Akian, R. A., "The Influence of Mounting Compliance and Operating Conditions on the Radial Stiffness of Ball Bearings: Analytic and Test Results," *Rotating Machinery and Vehicle Dynamics*, DE-Vol. 35, 1991.

[8]Walford, T. L. H., and Stone, B. J., "The Measurement of the Radial Stiffness of Rolling Element Bearings Under Oscillating Conditions," *Journal of Mechanical Engineering Science*, Vol. 22, No. 4, 1980, pp. 175–181.
[9]Ertas, B., "The Effect of Static and Dynamic Misalignment on Ball Bearing Radial Stiffness for Various Axial Preloads," M.S. Thesis, Mechanical Engineering Dept., Texas A&M Univ., College Station, TX, May 2001.
[10]Vance, J. M., and Shultz, R. R., "A New Damper Seal for Turbomachinery," *Vibration of Rotating Systems*, ASME DE-Vol. 60, Sept. 1993.
[11]XLTRC, Computer Code for Rotordynamic Analysis, Turbomachinery Lab., Texas A&M Univ.
[12]Schmidt, B., "The Experimental Determination of the Dynamic Radial Stiffness of an Angular Contact Ball Bearing," M.S. Thesis, Mechanical Engineering Dept., Texas A&M Univ., College Station, TX, May 2001.
[13]Feng, N. S., and Hahn, E. J., "Rolling Element Bearing Non-Linearity Effects," Rept. 1999, Univ. of New South Wales, Sydney, NSW, Australia, 1999.
[14]Yamamoto, T., "On the Critical Speeds of a Shaft," *Memoirs of the Faculty of Engineering*, Vol. 6. No. 2, 1954.
[15]Mitchell, J., "Machinery Analysis and Monitoring," Pennwell Books, Pennwell, Tulsa, OK, 1981, p. 518.